Research Article

Omar Bahattab, Ibrahim Khan, Sami Bawazeer, Abdur Rauf*,
Muhammad Nasimullah Qureshi, Yahya S. Al-Awthan, Naveed Muhammad, Ajmal Khan,
Muhammad Akram, Mohammad Nazmul Islam, and Talha Bin Emran

Synthesis and biological activities of alcohol extract of black cumin seeds (*Bunium persicum*)-based gold nanoparticles and their catalytic applications

https://doi.org/10.1515/gps-2021-0041
received April 20, 2021; accepted June 24, 2021

Abstract: Fast, simple, and environmentally friendly gold nanoparticles (Au-NPs) capped and stabilized with black cumin (*Bunium persicum*) seed alcohol extract are reported. The aqueous gold ions (Au^{3+}) were treated with *B. persicum* (BP) seed extract, which resulted in a rapid color change to red, indicating the synthesis of Au-NPs. UV-Vis spectroscopy, FTIR, SEM, energy dispersive X-ray (EDX), and X-ray diffraction (XRD) techniques were used to further characterize the Au-NPs. Its stability was assessed against various pH levels and sodium chloride levels (NaCl), different salts of same concentration as well as at a range of temperature (30–100°C). The UV-Vis spectrum in the Au-NPs produced a 540 nm plasmon surface resonance, and a 25–50 nm range of particulates was shown in the SEM analysis. In addition, the FTIR spectra confirmed the inclusion in the capping and decrease of Au-NPs of amines, amide groups, and alcohols. The EDX analysis confirmed the presence of element Au. Furthermore, Au-NPs were tested for enzyme inhibition and antibacterial and antifungal activities and showed remarkable response. These findings have concluded that BP seed extract is an effective bio-reductant of gold nanoparticle synthesis, which can be further applied in different biomedical and pharmaceutical industries.

Keywords: *Bunium persicum*, gold nanoparticles, stability of Au-NPs, antimicrobial, enzyme inhibitory activity

1 Introduction

Gold and silver nanoparticles in particular attracted significant attention in sensing, imaging, and biomedical devices [1]. Nanoparticles were synthesized using a variety of physical and chemical methods, all of which produce a large number of hazardous by-products. Nanotechnology has a gradually significant role in improving the design and performance in areas such as biomedical, electronics, equipment, agriculture, food, energy, and cosmetics and energy. Scientists and researchers in this field were attracted to the development and utilization of nanotools in a broad field in order to achieve numerous goals [2]. In the last few decades, nanotechnology obtained remarkable importance due to its application in catalytic, optical, electronic, and medicinal fields [3]. The application of nanotechnology in medicinal science is of most importance due to its beneficial impact on human as well as animal and plant health. Controlled drug delivery [4], tissue engineering [5], tumor detection and destruction [6], electroluminescence [7], drug and disease sensors [8,9],

* **Corresponding author: Abdur Rauf,** Department of Chemistry, University of Swabi, Swabi, Anbar, KPK, Pakistan, e-mail: mashaljcs@yahoo.com
Omar Bahattab: Department of Biology, Faculty of Science, University of Tabuk, Tabuk, Saudi Arabia
Ibrahim Khan, Muhammad Nasimullah Qureshi: Department of Chemistry, University of Swabi, Swabi, Anbar, KPK, Pakistan
Sami Bawazeer: Pharmacognosy Department, College of Pharmacy, Umm Al-Qura University, Makkah, Saudi Arabia
Yahya S. Al-Awthan: Department of Biology, Faculty of Science, University of Tabuk, Tabuk, Saudi Arabia; Department of Biology, Faculty of Science, Ibb University, Ibb, Yemen
Naveed Muhammad: Department of Pharmacy, Abdul Wali Khan University, Malakand, KPK, Pakistan
Ajmal Khan: Natural and Medical Sciences Research Center, University of Nizwa, P.O. Box 33, Birkat Al Mauz 616, Nizwa, Oman
Muhammad Akram: Government Post Graduate College Charsadda, Charsadda, KPK, Pakistan
Mohammad Nazmul Islam: Department of Pharmacy, International Islamic University Chittagong, Chittagong, 4318, Bangladesh
Talha Bin Emran: Department of Pharmacy, BGC Trust University Bangladesh, Chittagong, 4381, Bangladesh

and diagnosis of cancer through MRI [10] are some examples of nanoparticle application in medical fields. Catalyst has gained popularity in recent decades, particularly in academic and commercial synthetic processes. Interestingly, the confluence of nanoscience and chemistry led to nanocatalysts where many organic chemists were extremely intrigued to the vast surface areas and wide catalytic capabilities in a variety of catalytic actions [11,12]. Therefore, nanoparticle additives are proposed to avoid at least many of the detrimental effects of conventional stabilization methods due to their distinctive features as an emerging alternative stabilizer [13]. Currently, different techniques are applied for the synthesis of nanoparticles, including microwave-assisted synthesis [14], chemical and photochemical synthesis protocols [15], reduction in solution [16], and electrochemical synthesis route [17].

Green nanotechnology, a revolutionary branch of nanoscience, has developed into a significant study subject in various fields, including biology, water purification, and medicine [18,19]. Green chemistry principles are being used for the synthesis of nanomaterials, which is a relatively new emergent challenge in terms of sustainability. Metal and metal oxide nanoparticles have gained considerable interest in recent decades due to their several favorable features, including catalytic, optical, magnetic, and electrical properties [20,21]. The green synthesis of nanoparticles through eco-friendly synthesis methods is gaining attention among researcher community because they do not require high pressure, temperature, and toxic chemicals. In green nanotechnology, metal nanoparticles have been synthesized by the use of microorganism and macroorganism. The microorganisms that are used for the synthesis of metal nanoparticles are bacteria [22] and fungi [23], and plant extracts [24] are used for the synthesis of green nanoparticles. These biologic systems have the ability to synthesize nanoparticles in safe, easy, and economical way. Studies have found that many microorganisms can produce inorganic metallic nanoparticles including gold, silver, alloy, and others through either intracellular or extracellular routes. Fungus *Fusarium oxysporum*, *Verticillium* sp., and actinomycete synthesized gold nanoparticles extracellularly. Monodisperse gold nanoparticles have been synthesized by using alkalotolerant *Rhodococcus* sp. under extreme biological conditions like alkaline and slightly elevated temperature conditions. Gold nanostructures in different shapes (spherical, cubic, and octahedral) can be synthesized by filamentous cyanobacteria from Au(I)–thiosulfate and Au(III)–chloride complexes. Bacterium *Pseudomonas stutzeri* AG259 can be used to synthesize silver nanoparticles. Magnetotactic bacteria can synthesize intracellular magnetic particles of both iron oxide and iron sulfides. The palladium nanoparticles could be synthesized by the sulfate-reducing bacterium, *Desulfovibrio desulfuricans*, and mercury nanoparticles can be synthesized by *Enterobacter* sp. [25]. A large variety of secondary metabolites such as proteins, amino acids, polysaccharides, enzymes, vitamins, and organic acid are included in the extracts for metal NP biosynthesis, which helps to reduce metal ions and stabilize the NPs. $HAuCl_4$ which dissociates into Au^{3+} ions, whereas AuCl dissociates into Au^{+}, is one of the precursors of Au reduction. As Au^{+} is far less soluble than Au^{3+}, it was not so widely examined. However, its solubility can be increased by the formation of coordination complexes with alkenes, alkanethiols, alkylamines, alkylphosphines, and various anions. Research has demonstrated that, in the early phases of Au^{+} biofabrication, the Au^{+} concentration originally increased but then declines when Au^{0} began to emerge, suggesting that Au^{3+} is first converted to Au^{+} and subsequently to Au^{0}. It was believed that the reduction from Au^{+} to Au^{0} is a single-phase process, compared to many chemical transformations from Au^{3+} to Au^{0} [26]. In the current study, Kala zeera (*Bunium persicum* Bioss.), in Figure 1, was used for the synthesis of Au-NPs. This plant material was selected based on its indigenous medicinal importance and use [27]. The high qualities of BP herbal spices are widely used for culinary, perfume, and carminative industries [28], while its medicinal value is represented world-

Figure 1: Black cumin (*Bunium persicum*) seeds.

wide with various names. *B. persicum* seeds are used for stimulants and carminatives and are used by indigenous people to treat diarrhea and dyspepsia [29], while the extracts are hypoglycemic and can be used for the treatment of diabetes and obesity. The ripe zeera seeds contain an essential oil content of monoterpene aldehyde (5–14%). The primary components include cumin aldehyde, *p*-mentha-1, 3-dien-7-al, *p*-mentha-1, and 4-dien-7-al [30–32]. The use of plant-based nanoparticles for the removal of toxic materials from waste water has the benefit of being of eco-friendly nature, easy to be synthesized, and readily accessible substrates. Wastewater generated from industrial processes contains various toxic compounds such as dyes, phenolic compounds, antibiotics, pesticides, detergents, and spent petroleum products [33,34]. Current treatment methods like activated carbon adsorption, microbial degradation, photo catalytic degradation, electro-Fenton method, electro coagulation, and electrochemical treatment are not efficient for the complete removal of these toxic substances [35]. This research was intended to synthesize green Au-NPs for their antibiotic, antifungal, and catalytic application.

2 Materials and methods

2.1 Materials

Dry seeds of black cumin (*B. persicum*) were obtained from local market. The analytical grade was uncovered for all chemicals and reagents in this study. Hydrogen tetrachloroaurate trihydrate ($HAuCl_4 \cdot 3H_2O$), methanol, and sodium chloride were obtained from Merck, Germany.

2.2 Extraction

Known weight (1,000 g) of dry seeds of black cumin (*B. persicum*) was soaked in 2 L of alcohol/methanol for 7 days followed by rotary extraction. The methanol extract was concentrated at 50°C to produce a dark-brown residue under reduced pressure. Around 1 g of the obtained extract was diluted with 100 mL of deionized distilled water and stored in a refrigerator at 5°C for further use.

2.3 Synthesis of gold nanoparticles

Different ratios of 1 mM $HAuCl_4$ and black cumin extract were used to synthesize Au-NPs. In a typical method, a known amount of black cumin extract was added to 1 mM warm gold solution ($HAuCl_4$) under vigorous stirring for 4 h. Stirring was stopped when the color shifted from yellow to red and then dark red as shown in Figure 2.

2.4 Kinetic study and stability of Au-NPs

In order to find the time-dependent synthesis of Au-NPs, kinetic study was performed. In such study, samples were

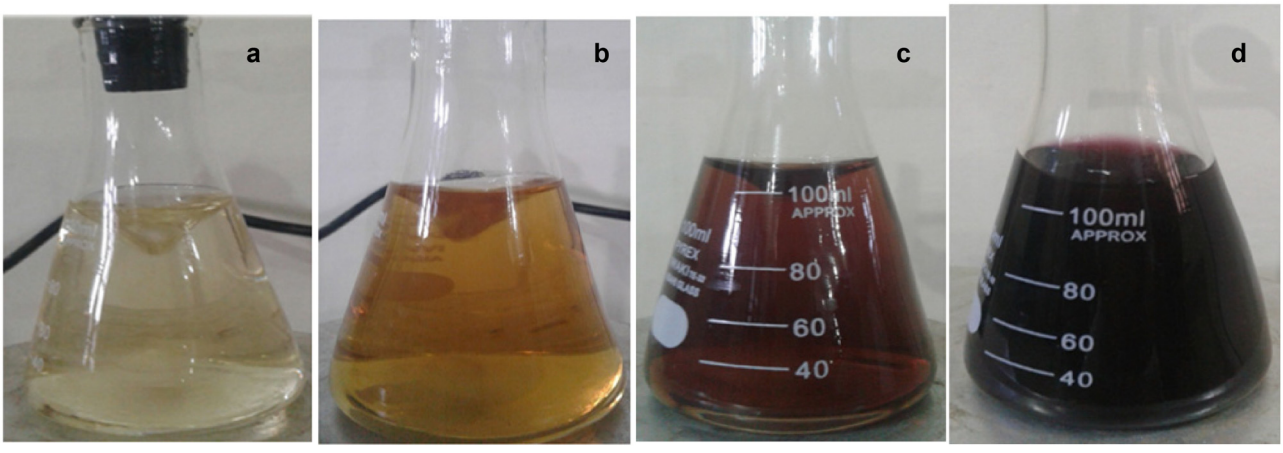

Figure 2: Color change of Au-NPs of Black cumin (*Bunium persicum*) synthesis with time. (a) Gold solution, (b) initial mixing of gold solution and extract, (c) after 30 min, (d) after 4 h.

drawn from reaction mixture after a certain interval of time and UV data were recorded periodically. The stability of Au-NPs was checked through varying the parameter conditions like pH, type of salt, concentration, and temperature. The pH of Au-NP solutions was adjusted between 2 and 14, due to the drop-wise addition of 1 M HCl or NaOH solution. The effect of sodium chloride (NaCl) on the stability of Au-NPs was determined by adding (1 mL) 0.1–1.5 M NaCl to the biosynthesized Au-NPs (2 mL). Similarly, the effect of other salt with same concentration (0.1 M) was also checked. UV-Vis spectrum was obtained after each treatment. The temperature effect on the stability of Au-NPs has been examined each time by heating Au-NPs for 30 min at 30°C, 50°C, and 100°C in the water bath [36].

2.5 Catalytic activity of Au-NPs

Reaction studies were carried out to check the catalytic action of synthesized Au-NPs. In the presence of NaBH4 and Au-NPs, aqueous methylene blue (MB) is reduced to Leuco MB (LMB). Au-NPs act as electron relay and initiate shifting of electron from BH_4^- ion (donor B_2H_4/BH_4^-) to acceptor (acceptor LMB/MB) and thus causing reduction of the dye. The maximum absorption in aqueous media is 664 nm and the shoulder peak 615 nm. The reaction was observed with UV-Vis spectroscopy at room temperature and ranges from 200 to 700 nm [37].

2.6 Antibacterial activity

The activity of BP and Au-NPs was carried out using the agar well diffusion method [38]. A medium for the antimicrobial activity was Mueller–Hinton Agar. After that, 1 mL of the broth inoculums of the test bacteria was applied with the help of sterile micropipette and spread equally by the sterile rod spreader of glass, and at room temperature, plates are allowed to dry. Each well plate was subsequently bored 6 mm in diameter. The samples with 66 µL of DMSO (3 mg/mL) were added to each well using sterilized micropipette and permitted for diffusion for 2 h. Specified quantities of both of the tested samples were used. Then the plates were incubated at 37°C for 24 h and the zone of inhibition was calculated in diameter (mm). Amoxicillin and norfloxacin were used as standard antibiotics.

2.7 Antifungal activity

A standard procedure was used to evaluate the antifungal properties of BP and Au-NPs [39]. The fungal inhibition potential of the extracts and synthesized nanoparticles had been assessed with the tube dilution test. In order to prepare a stock solution, each compound was dissolved with DMSO at 2 µg/mL. The SDA (Sabouraud dextrose agar, 4 mL) was poured into each tube and autoclaved for 15 min at 120°C, then cooled down to 15°C. Stock solution (66.6 µL) was added with SDA medium to provide 2 mg/mL with the final concentration. In addition, all tubes could solidify at room temperature in a slanting position. Then, each tube has been incubated with inoculum from a fungal cultivation lasting for 7 days. After 7 days of incubation, the antifungal activity was observed for each sample and standard drug. Triplicate antifungal activity was carried out in this study. The results were then analyzed to calculate the visible fungal growth and the percentage of activity.

2.8 Urease inhibitory activity

Au-NPs together with an extract of *B. persicum* have been screened for urease enzyme inhibition. For measuring urease-II inhibition, the test solutions were incubated with urea [40]. In this method, indophenol was used as a urease enzymatic activator for ammonia production, whereas thiourea as a standard inhibitor. The urease (25 µL of 0.25 mg/mL) and samples to be tested were incubated under standard conditions in 96-well plate. The substrate (urea) was added to the experimental solution after incubation and then again incubated. The absorbance of incubated mixture was measured at 630 nm to get the reread data. Each well was supplemented with 45 phenol reagents (1% w/v), NaOH (0.005% w/v), 70 µL alkali reagent (0.5% w/v), sodium nitroprusside, and 0.15% active chloride. The post data were noted after incubation for 50 min. The inhibition percentage was calculated with the following formula:

$$\% \text{ Inhibition} = 100 - (\text{OD test well}/\text{OD control}) \times 100. \quad (1)$$

2.9 Xanthine oxidase (XO) activity

The BP and Au-NPs were tested for XO inhibitory activity using our previously published experimental procedure [41].

The antagonistic effect of both of the samples was quantified spectrophotometrically. The solution of allopurinol was prepared through mixing of 5.0 mg allopurinol in 5 mL of 0.15 M phosphate buffer with a pH of 7.5. The solution of XO was prepared by diluting 30 µL of a 5.0 U/0.2 mL XO, making 3.0 mL as the final volume. The xanthine solution was prepared by addition of five drops of 1.0 M NaOH to 22.7 mg xanthine and dissolution occurred with deionized water, making the final volume as 250 mL. The BP and Au-NPs were dissolved in DMSO up to 1 mg/mL final concentration. The total volume of assay mixture was 3.4 mL, consisting of BP (0.3 mg) and Au-NPs (0.25 mM), 0.15 M buffer, and 100 µL of 0.03 U/mL XO solutions. The mixture was incubated at normal temperature for 10 min. Finally, the reaction began by adding 1 mL of a 0.6 mM xanthine solution and mixing well. The absorption readings were measured at 295 nm to demonstrate a reaction (uric acid formation). The positive control (allopurinol) was used up to 0.2 µM in the assay mixture. The percent inhibition was calculated for each tested sample.

2.10 Carbonic anhydrase activity

Both of the samples were tested for CA-II antagonistic effect. To find the interaction of our samples with reaction mixture, the following reagents were used. The complete mixing volume was 200 µL in a well contained 140 µL (20 mM HEPES, Bioworld – cat# 40820000-1), Tris (Invitrogen – cat# 15504-020) buffer (pH 7.4), 20 µL of the enzyme (from bovine; Sigma-Aldrich, C2624, PCode: 1001584424), and 20 µL (0.5 mg/mL in dimethyl sulfoxide) of both samples, which were mixed and incubated at 25°C for 15 min. Besides, a pre-read datum was taken after inoculation at 400 nm and then 20 µL substrate, 4-nitrophenyl acetate, colorless was formed. Then it transformed into 4-nitrophenol and carbon dioxide during hydrolysis. During this experiment, 4-nitrophenol, a yellow-colored compound, was formed. The reaction took place at 25–28°C, while acetazolamide was applied as a standard for this experiment and triplicate analysis was measured [42].

2.11 Statistical analysis

The data were expressed as mean ± standard error of the mean (SEM). ANOVA was followed by Dennett's test using GraphPad Prism 8.0 (GraphPad Software Inc., San Diego CA, USA).

3 Results

3.1 Selection of Au-NPs and extract ratio

Results of Figure 3 showed the UV-Vis spectrum of different ratios of gold and extract solution. The graph almost showed similar peaks in the range of 540–550 nm. By varying the ratio of gold and extract, the peak intensity changed. The sharpness of the peaks shows the uniformity of Au-NPs. Based on peak sharpness and intensity, the best ratio of 25:1 was selected due to its more uniform peak at 540 nm.

3.2 Kinetic study of Au-NPs

Figures 4 and 5 show kinetic study of Au-NPs. The number and uniformity of nanoparticles increased with passage of time. The regression analysis showed $R^2 = 0.9895$, while the rate of reaction was 5.9807×10^{-3}.

3.3 Stability toward pH

In order to understand the effect of pH on the stability of Au-NPs, the pH of Au-NP solution was adjusted between

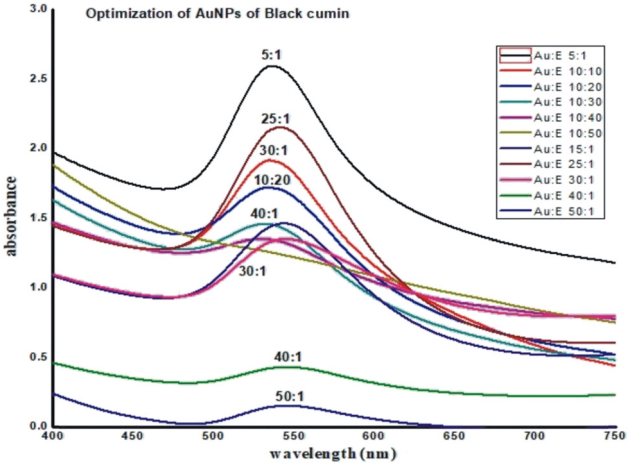

Figure 3: Comparison of UV-Vis spectra for different ratios of gold and extract solution.

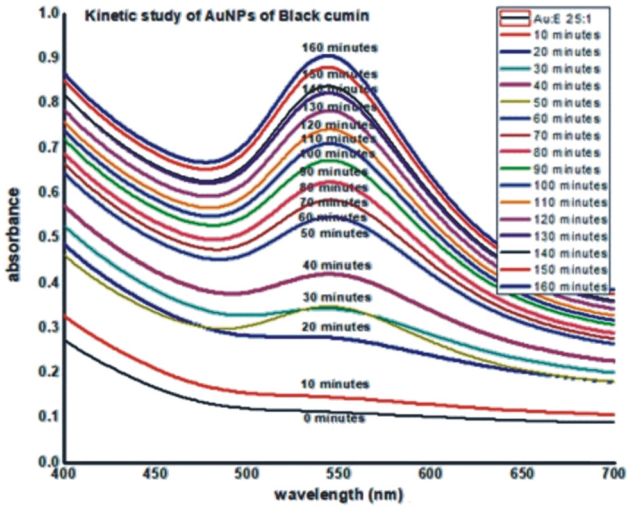

Figure 4: Comparison of UV-Vis data for kinetic study on Au-NPs of black cumin (*Bunium persicum*).

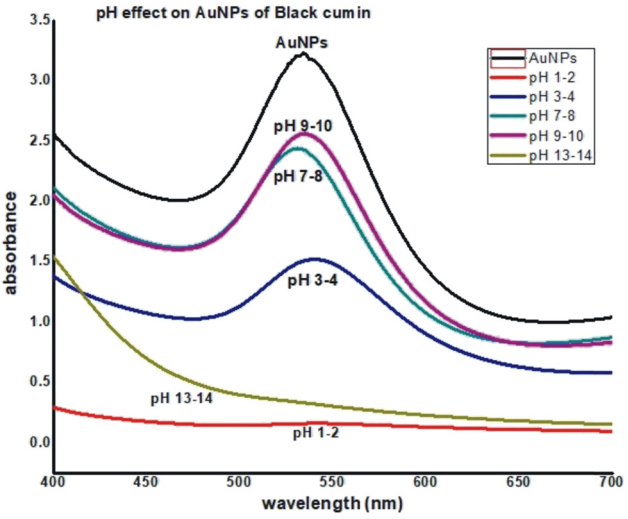

Figure 6: Comparison of UV data of Au-NPs at different pH.

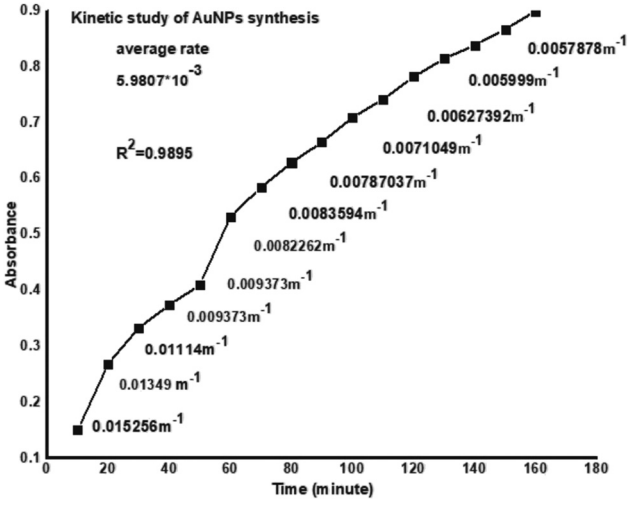

Figure 5: Comparison of kinetic study of synthesis of Au-NPs.

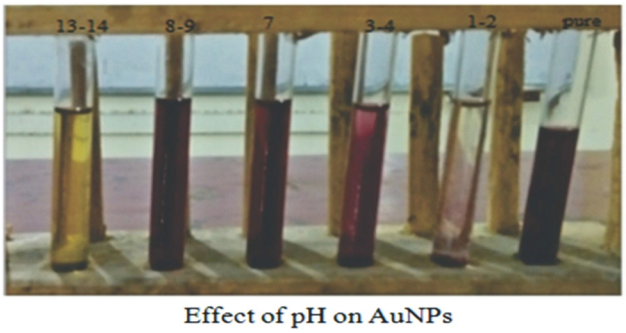

Figure 7: Comparison of stability of Au-NPs at different pH.

1 and 14; the solution was kept for 24 h at room temperature and the effect was obtained by recording UV-Vis spectra. The results showed that the Au-NPs were more stable between 3 and 12 pH range, while lower stability was observed toward more acidic and basic, i.e., 1–2 and 13–14. Such conclusions were drawn from the absorbance value found at different pH, as shown in Figure 6. The reason of instability of Au-NPs at lower and higher pH may be due to the removal of stabilizer (plant extract) from the gold surface to destabilize the nanoparticles. Moreover, very low pH caused the reoxidation of neutral Au-NPs. Furthermore, the change in pH also altered the color of the Au-NPs which is due to the removal of stabilizer, as displayed in Figure 7. However, improved stability of alkaline pH (8–10) was observed. Moderate stability of the Au-NPs was obtained at other pH values, i.e., 3–4, where red shifting and peak expansion show from the nanoparticles [17].

3.4 Stability toward salt

The effect of salt NaCl on Au-NPs of *B. persicum* was determined by varying the salt concentration (0.1–1.5 M) on synthesized Au-NPs. After 24 h of intermixing salt with Au-NPs, aggregation of Au-NPs started which was fixed from a decline in absorption of the UV-Vis spectra. In addition, an increasing amount of the salt concentration shows a gradual color change of the Au-NPs. The addition of NaCl (strong electrolyte) protects against the negative charges of colloidal gold nanoparticles and causes to clump into greater aggregates. This can be concluded from the results that high salt concentration could destabilize the nanoparticles by removing the stabilizer, as exhibited in Figures 8 and 9.

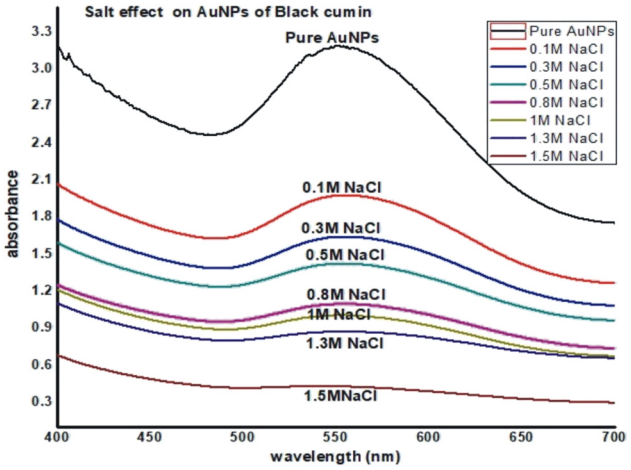

Figure 8: Effect of salt NaCl on Au-NPs of *Bunium persicum* after 24 h.

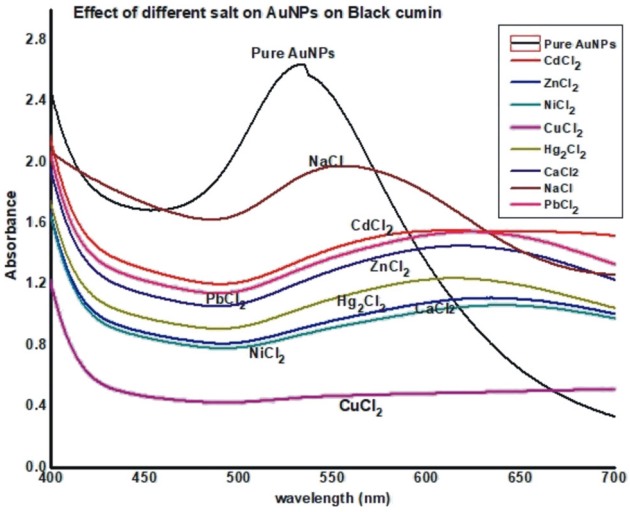

Figure 10: Comparison effect of different salts on Au-NPs.

Figure 9: Effect of salt (NaCl) on Au-NPs of *Bunium persicum*.

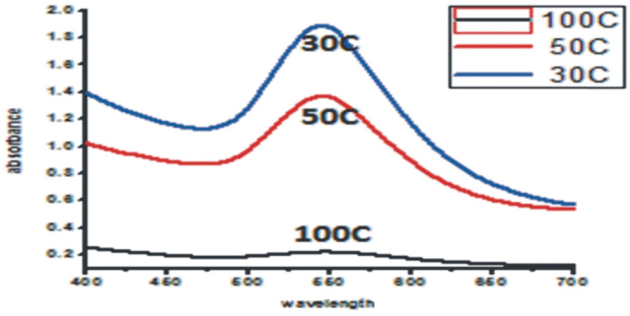

Figure 11: Comparison effect of heat on Au-NPs.

3.5 Stability effect on different salts

The effects of different salts (NaCl, $CaCl_2$, $CuCl_2$, $NiCl_2$, Hg_2Cl_2, $PbCl_2$, $ZnCl_2$, and $CoCl_2$) on Au-NPs of *B. persicum* were determined by keeping the salt concentration constant (0.1 M). After 24 h of mixing salt solution with Au-NPs, it was observed that the salts cause the destabilization of nanoparticles by shielding the negative charges of the colloidal gold nanoparticles and causes to clump together to form larger aggregates which are obvious from decrease in the absorbance and broadness of peak of solution, as displayed in Figure 10.

3.6 Stability effect on heat

The stability of Au-NPs was explored with the heating of the solution of nanoparticles during 30 min at a range of 30–100°C. The Au-NPs showed remarkable thermal instability at high temperatures in Figure 11. The change in UV-Vis intensities could have been clearly demonstrated in that the Au-NPs become destabilized at high temperature, i.e., 100°C.

3.7 Catalytic activity of Au-NPs

The absorbance at maximum wavelength (664 nm) with time was followed spectrophotochemically. The intense blue color of the methylene blue solution faded and became colorless during degradation process (Scheme 1). Addition of biosynthesized Au-NPs improved the reduction process (dye degradation up to 95% within 14 min), as exhibited in Figures 12 and 13.

3.8 Characterization of Au-NPs

The synthesis of Au-NPs was tracked by the UV-Vis spectrum solution with a wavelength between 200 and

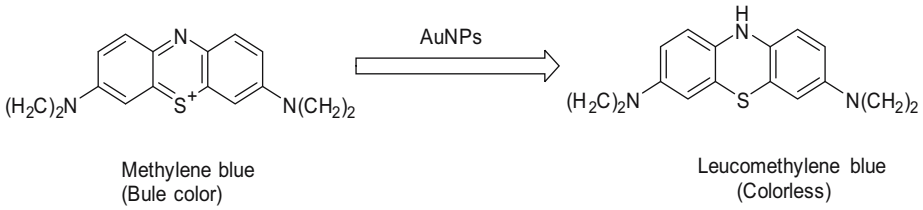

Scheme 1: Catalytic degradation of methylene blue.

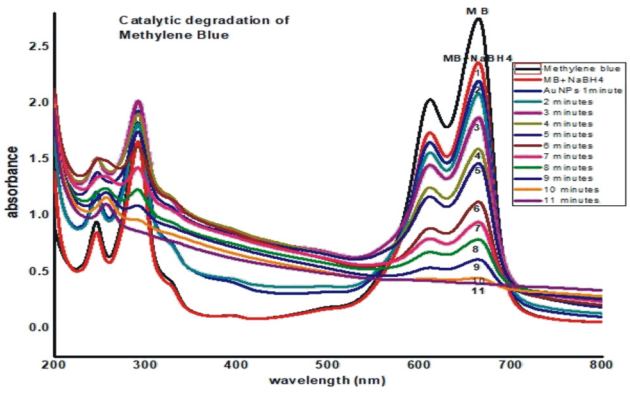

Figure 12: Comparison of UV data of catalytic degradation of methylene blue.

900 nm in 10 mm optical path-length quartz cuvettes with a UV-Vis spectrophotometer (Shimadzu UV-1800 Japan). The size of Au-NPs was characterized by AFM and SEM techniques. Energy dispersive X-ray (EDX) (INCA-200, England) study was carried out for elemental analysis, thermogravimetric analysis (TGA) for thermal stability, and X-ray diffraction (XRD) for crystallinity of Au-NPs.

The nanoparticle solution has been centrifuged for Fourier transform infrared spectroscopy (FTIR) measurements at 10,000 rpm for 15 min to discard the free proteins or other elements remaining in the product solution. The samples were vacuum-dried and finally broken using the mortar with the split KBr, which led to the formation of the KBr pellets for measuring in the FTIR (Prestige 21 Shimadzu) instrument sample holder. The crude extract FTIR spectra showed broader bands at 3,365/cm, which are a characteristic zone of O–H stretch, H-bonded of alcohols and phenols or amine group, compared to that from Au-NPs of *B. persicum* extract which shift to 3,280. A long narrow band was seen at the wave number of 2,930/cm and indicated the presence of C–H stretch of alkane groups. Weak bands were noted at 1,460/cm and represented the N–O symmetric stretch nitro groups. Very weak bands were formed at 1,243 and 1,026/cm, corresponding to C–N stretch aromatic amines and aliphatic amines, respectively. The peak at 3,280/cm corresponded to O–H group of carboxyl, while that at 1,630/cm corresponded to N–H stretch of primary amines in AuNP spectrum. Similarly, the striking vibration of aliphatic

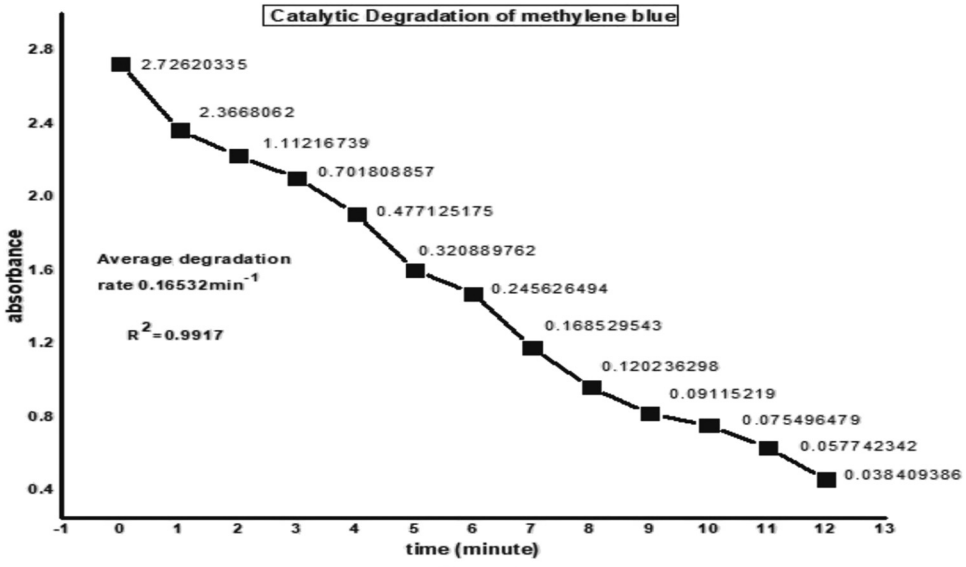

Figure 13: Comparison of kinetic study of catalytic degradation of methylene blue by Au-NPs.

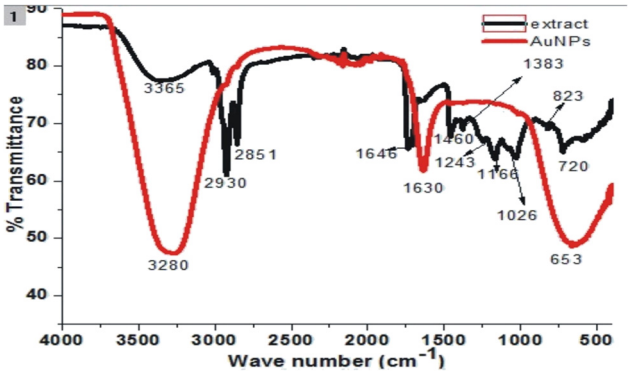

Figure 14: Comparison of FTIR spectra of *Bunium persicum* (black cumin seed) seed alcohol extract and Au-NPs.

amines, alcohols, or phenols at 1,026/cm corresponds, and the strip at 1,646/cm indicates the presence of the functional carbonyl group of the amide protein linkage, as shown in Figure 14.

The SEM images show *B. persicum* Au-NPs in size from 25 to 50 nm. Nanoparticles of different sizes are nearly spherical in form. However, small numbers of anisotropic nanostructures, such as nanorods, nanotriangles, and several polygonal nanoprisms, have also been noted. Moreover, the presence of Au in the samples was shown by the EDX study. In Au-NPs, strong signals from Au atom were observed at around 2 keV, while in 9.7, 10.2, and 11.7 keV weak signals were observed. The presence of strong C and O signals was also due to the presence of biomolecules involved in the Au-NP cap and exposed in Figures 15 and 16.

The XRD is a common and precise technique used to identify molecular structures and the level of crystallinity of synthesized NPs. By using XRD patterns, they confirmed the size of those green Au-NPs as shown in Figure 17. In this experiment, the XRD peaks at $2\theta^{\circ}$ = 29.9(466),

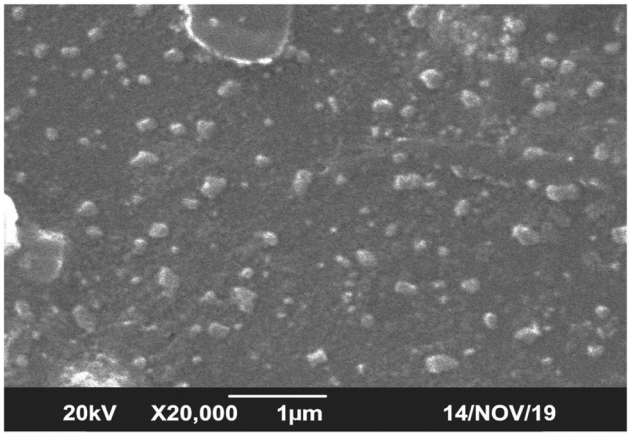

Figure 15: SEM images of *Bunium persicum* of Au-NPs.

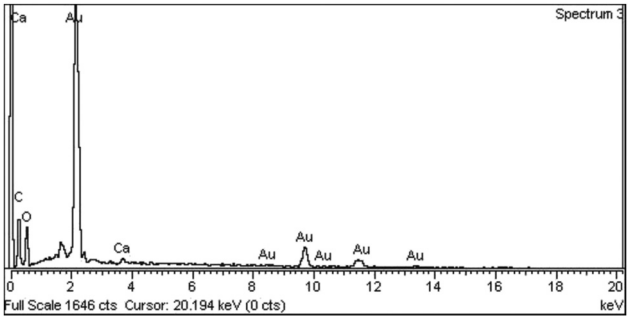

Figure 16: EDX spectra of Au-NPs of *Bunium persicum*.

33.15(699), 36.15(3,207), 39.35(2,765), and 49.4(890) indicate the formation of BP-based solid Au-NPs. These peaks also show the same agreement of Au-NPs peaks as reported in the literature for Au-NPs. These broadened diffraction peak values of Au-NPs indicate that the green synthesized Au-NPs have smaller size. Some other unknown crystalline peaks at 20°, 58.75°, and 62.25° were appeared in the XRD patterns; the peaks which show that some crystallized biomolecules are present in solid Au-NPs which are made by *B. persicum* plant extract. The Au-NP average size was calculated by using Scherer's equation that is 25–50 nm.

B. persicum of Au-NPs (7.5 mg) was heated in alumina crucibles for thermal stability and TGA profiles were recorded at the scan speed of 100°C/min in the nitrogen atmosphere from 0°C to 600°C. Different weight losses for Au-NPs were observed within the same temperature range. The loss of entrapped water molecules from the polymer matrix in the range 100–150°C was observed as first decrease in sample weight. The resulting weight loss could be due to the thermal disintegration of the polymer and the polymer that stabilizes NPs from 200°C to 300°C, while the residual polymer may be converted to carbon residues as the third weight loss.

The size and morphology of Au-NPs were found by atomic force microscopy. The AFM images showed that the particles have average size of 25–50 nm, as shown in Figures 18 and 19.

3.9 Antimicrobial activity

3.9.1 Antibacterial effect

B. persicum extract and Au-NPs were tested and showed no antibacterial activity against *Acinetobacter baumannii*, *Providencia stuartii*, and *Streptococcus aureus*. However, *B. persicum* showed moderate zone of inhibition (20 mm)

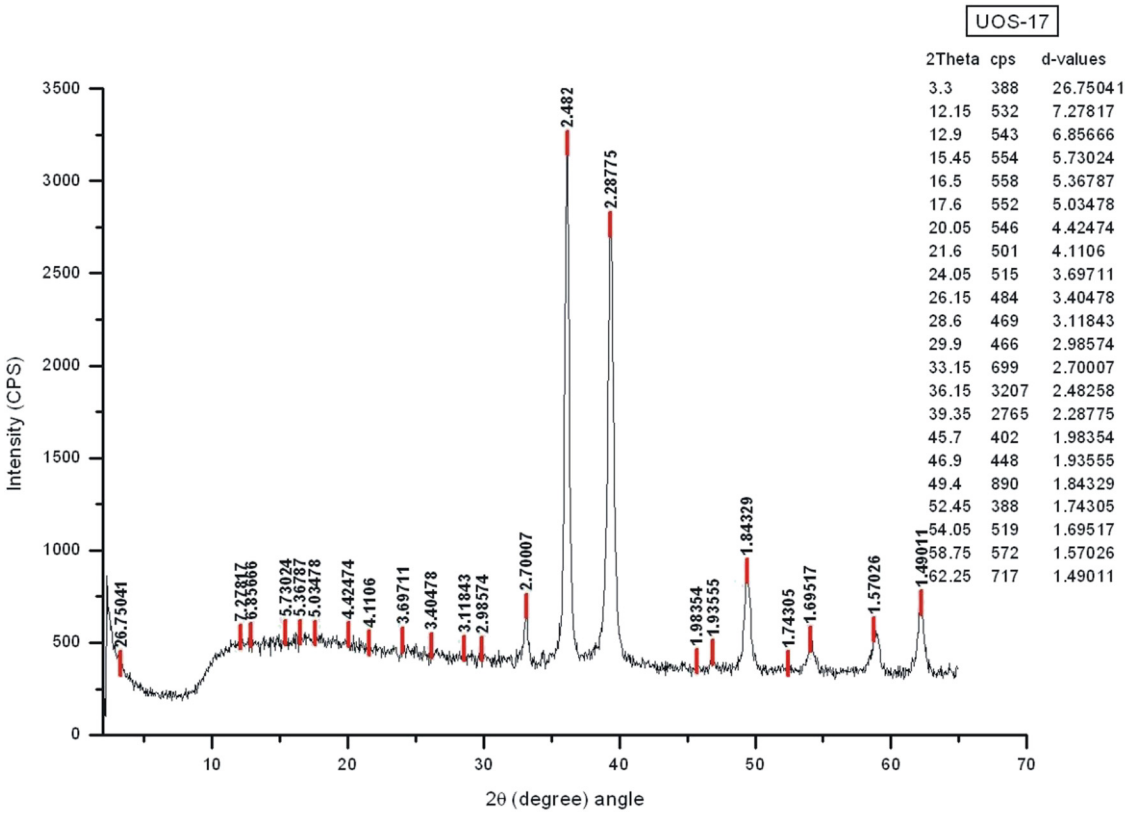

Figure 17: XRD image of Au-NPs of *Bunium persicum*.

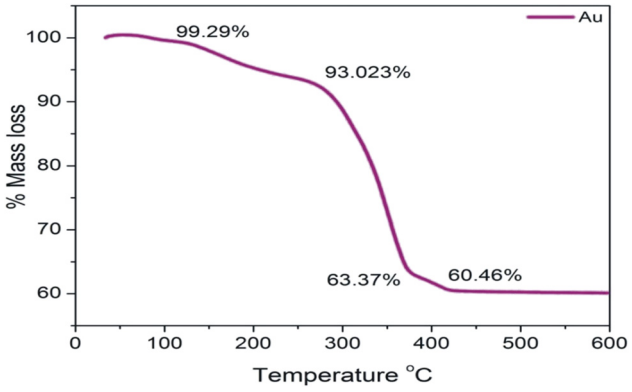

Figure 18: TGA spectrum of *Bunium persicum* Au-NPs.

compared with standard against *E. coli*. Analyses were performed in triplicate and are shown in Table 1 and Figure 20.

3.9.2 Antifungal effect

The Au-NPs were also screened against the three fungal strains. Antifungal activity with BP extract is shown in Table 2 and observed moderate antifungal activity compared with control.

3.10 Enzyme inhibition activity

3.10.1 Effect on urease

The extract of BP and Au-NPs were tested against urease as presented in Table 3. The inhibitory potential of Au-NPs was better than that of BP with percent inhibition of 93.11 and 45.98, respectively.

3.10.2 Effect on XO

The extract of BP and Au-NPs demonstrated significant XO inhibition effect as shown in Table 4. The percent effect of BP and Au-NPs was 80.76 and 94.28, respectively. The inhibitory potential of Au-NPs was near to allopurinol 97.66%.

3.10.3 Effect on carbonic anhydrase

The comparative study of BP extract and Au-NP result showed a promising inhibition. The inhibitory potential of Au-NPs was 86.87% as compared to the BP 62.98%, as presented in Table 5.

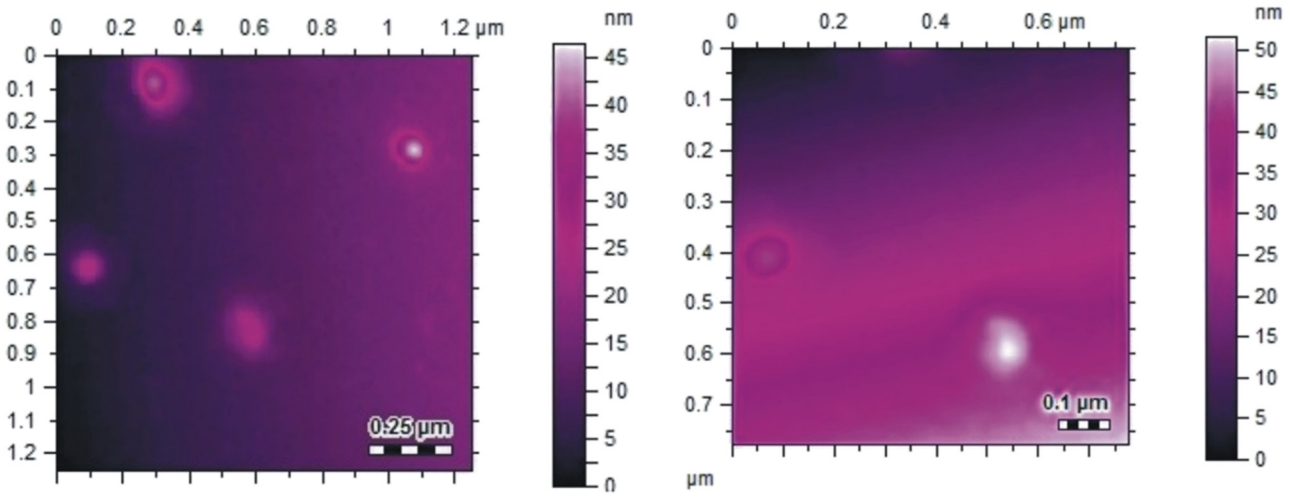

Figure 19: AFM images of Au-NPs of *Bunium persicum*.

Table 1: Antibacterial effect of BP and Au-NPs (zone of inhibition)

Bacterial strain	Zone of inhibition (mm)			
	BP	Au-NPs	Amoxicillin	Norfloxacin
Acinetobacter baumannii	NA	NA	25.34 ± 0.76	38.44 ± 0.88
Providencia stuartii	NA	NA	16.22 ± 0.65	27.87 ± 0.76
Streptococcus aureus	NA	NA	20.09 ± 0.88	37.59 ± 0.34
Escherichia coli	20	NA	30.87 ± 0.32	19.65 ± 0.23

Values are expressed as mean ± SEM of three different experiments. NA = not active; BP: *Bunium persicum*; Au-NPs: gold nanoparticles.

4 Discussion

Over three-quarters of the world's population receives healthcare from plants and plant extracts. Natural medicinal herbs are widely utilized across the world to treat chronic illnesses, ranging from acute to severe. Notwithstanding advances in technology and modern medicine, a significant portion of the global population continues to rely on herbal medicine [43–45]. That is why the scientific studies of these therapeutic agents are utmost essential to find out the primary actions along with side effects. A single plant extract or fraction accumulating thousands of molecules having agonistic and antagonistic effects is the major cause that these traditional medicines have multiple indications [46].

The pharmacodynamics of these agonistic molecules is attributed to the enzymes activating or inhibitory effects. The testing of these plants against various enzymes not only provides scientific background to the folklore of herbs but also guides the phytochemical scientist for *in vivo* studies. *B. persicum* is a food material, but is full of different therapeutic potentials such as epilepsy, antispasmodic, anti-inflammatory, antioxidant, etc. [34]. The main indicator that this metal nanoparticle is biosynthesized successfully is the change of solution color. Thus, due to the bioreduction of gold ion, fast changes of gold, from pale yellow to dark red, were observed. However, the antibacterial effect is especially reported against *E. coli*, indicating the use of these herbal agents for the treatment of urinary tract infection. *B. persicum* reported moderate antibacterial activity in comparison with amoxicillin and norfloxacin. Invasive candidiasis is a significant fungal infection in healthcare reported by several *Candida* spp.; *Candida albicans* are the most common species, but they vary considerably in proportion to the geographic location [47]. The disease ranges from minimal symptomatic candidaemia to fulminant sepsis with associated mortality of more than 70%. *Candida* spp. is a commonly used commensal organism in the skin and gut microbiota, as well as an invasive disease caused by disruption of skin and gastrointestinal barriers [48]. The antifungal activity of nanoparticles against *Aspergillus niger* and *Candida albicans* also showed positive results. A deeper knowledge of the specific *Candida* spp. virulence factors, host immune reaction,

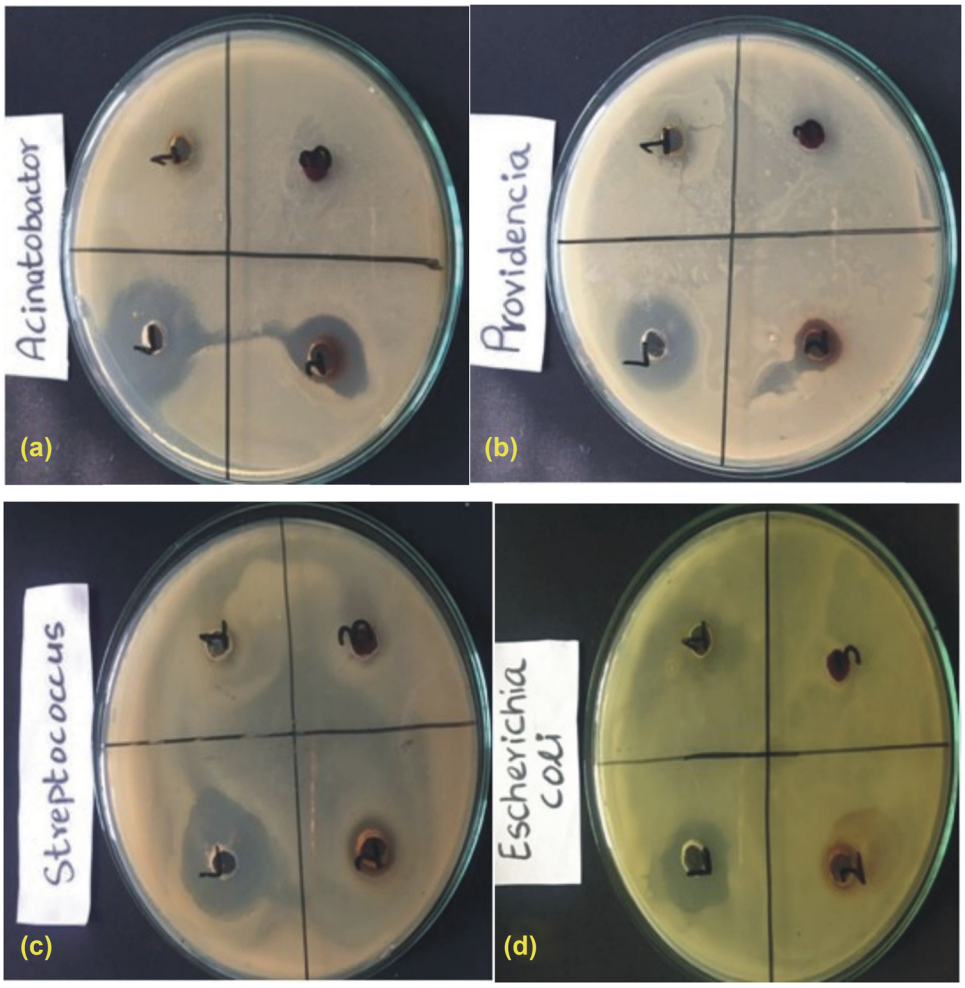

Figure 20: Antibacterial activity of extract and Au-NPs: (a) *Acinetobacter*, (b) *Providencia*, (c) *Streptococcus*, and (d) *Escherichia coli*.

Table 2: Antifungal effect of BP and Au-NPs (zone of inhibition)

Fungal strain	Zone of inhibition (mm)		
	BP	Au-NPs	Miconazole
Alternaria solani	NA	NA	100 ± 0.00
Aspergillus niger	20.67 ± 0.00	20.87 ± 0.00	100 ± 0.00
Candida albicans	100 ± 0.00	100 ± 0.00	100 ± 0.00

Values are expressed as mean ± SEM of three different experiments. NA = not active; BP: *Bunium persicum*; Au-NPs: gold nanoparticles.

Table 3: Effect of BP and Au-NPs against urease

Samples	Concentration (mg/mL)	% Inhibition	IC_{50} SEM (µg/mL)
BP	0.2	45.98 ± 1.56	—
Au-NPs	0.2	93.11 ± 1.99	29.98 ± 1.21
Thiourea	0.2	94.95 ± 1.87	21.23 ± 0.12

Values are expressed as mean ± SEM of three different experiments. BP: *Bunium persicum*; Au-NPs: gold nanoparticles.

and genetic sensitivity at the host level has given a significant insight into the development of early intervention strategies [49].

The bactericidal activity of transition metal NPs can be attributed to many different properties, the most important being the ability to generate reactive oxygen species (ROS) and their affinity to associate closely with R-SH groups as shown in Figure 21. The heavy metal ions can easily bind to SH groups, such as in cysteine, which can directly disrupt the function of specific enzymes or break S–S bridges necessary to maintain the integrity of folded proteins, causing detrimental effects to the metabolism and physiology of the cell. The generation of ROS is particularly destructive to bacterial cells as ROS are species of oxygen that are highly reactive and are produced during basic

Table 4: Effect of BP and Au-NPs against xanthine oxidase

Samples	Concentration (mg/mL)	% Inhibition	IC_{50} SEM (µg/mL)
BP	0.2	80.76 ± 0.65	96.09 ± 1.65
Au-NPs	0.2	94.28 ± 0.68	38.92 ± 0.94
Allopurinol	0.2	97.66 ± 1.54	0.59 ± 0.01

Values are expressed as mean ± SEM of three different experiments. BP: *Bunium persicum*; Au-NPs: gold nanoparticles.

Table 5: Effect of BP and Au-NPs against carbonic anhydrase

Samples	Concentration (mg/mL)	% Inhibition	IC_{50} SEM (µg/mL)
BP	0.2	62.98 ± 3.02	89.59 ± 2.87
Au-NPs	0.2	86.87 ± 2.98	43.98 ± 2.00
Acetazolamide	0.2	89.01 ± 1.54	18.90 ± 1.45

Values are expressed as mean ± SEM of three different experiments. BP: *Bunium persicum*; Au-NPs: gold nanoparticles.

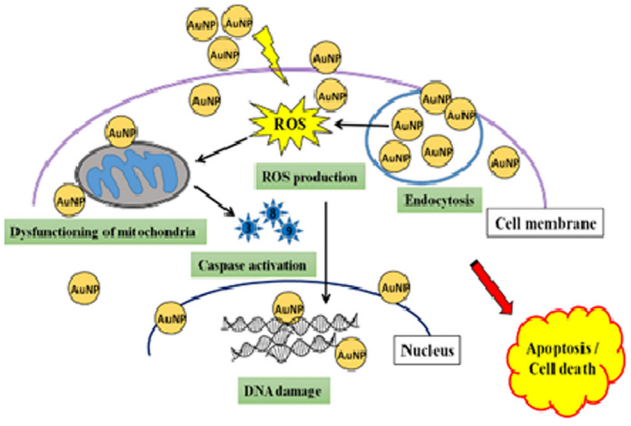

Figure 21: Mechanism of antibacterial action of AuNPs.

metabolism. Under high levels of stress, the levels of ROS can increase significantly, and it is hypothesized that their generation is one of the focal NP mechanisms of action that inhibit bacterial growth. ROS are produced when oxygen transforms into free radicals, superoxide, and peroxides, rather than water. A stress on the cell, such as UV light, DNA damage, and NPs, can cause ROS production to increase to a level that is toxic to the cell and can cause cell damage or cell death. It is observed that small NPs tend to be more toxic than large NPs due to larger surface area to volume ratio as compared to larger NPs. This can greatly increase the production of ROS which consequently can damage and inactivate essential biomolecules, including DNA, proteins, and lipids. Moreover, NPs are hypothesized to be able to participate in subcellular reactions as their size is comparable to biological molecules, i.e., large protein complexes. Another important factor in antibacterial activity is the charge of the NP. Positively charged NPs, such as amino-functionalized polystyrene particles, were able to alter the function of the electron transport chain in bacteria. More importantly, a positive charge in the NPs has been shown to enhance toxicity because the negative charge of the bacterial cell wall electrostatically attracts the positively charged NPs, causing them to be more effective [56].

Urease is functionally related to amidohydrolases and phosphodiesterase and found in various bacteria, fungi, and plants [50]. These enzymes are functionally breaking the urea into ammonia and carbon dioxide. The ammonia neutralizing the stomach acid provides healthy medium to *H. pylori*. This neutralization helps to the pathogenesis of *H. pylori* to peptic ulcer [51]. This *H. pylori* urease induced hyper-ammonia in stomach. The resulted induced ammonia got absorbed and caused hepatic inflammation and hepatic encephalopathy (HE). In addition to the peptic ulcer, urease also improves the urinary tract infection and crystallization of kidney stone. When ammonia is induced from the hydrolysis of urea due to microbial urease, the pH of urinary tract increases and this alkalization creates stone crystallization [52]. The significant urease inhibitory action of BP and Au-NPs strongly supports the use of BP in the management of gastrointestinal and urinary disorders. The urease inhibitors are suggested as antiepileptic [53] and the significant antagonistic effects of this plant approve the use of this herb in treatment of epilepsy and convulsion which are the pharmacological uses of BP [34]. The availability of ureases improves the liver dysfunction and therefore the urease inhibitors are the adjuvant therapeutic agents for the treatment or management of liver dysfunction. The BP and Au-NPs due to their strong urease inhibitors are strongly recommended for the treatment of said dysfunction. The liver dysfunctions are mainly caused by inflammatory and oxidative agents. Interestingly, our tested samples are used as anti-inflammatory, antioxidant, and liver protective [54]. The current urease inhibitory potential is strongly suggesting the use of BP in the effects.

XO belongs to the xanthine oxidoreductase enzyme family, accelerating the generation of ROS and production of uric acid. These ROS are responsible for inflammation and lot of other diseases [55], while uric acid causes gout. These ROS-related disorders might be treated with XO inhibitors. The XO inhibitors are considered as antioxidants because they stop the production of ROS.

The XO inhibitory potential of BP and Au-NPs means that they might be good anti-inflammatory, antioxidant, and analgesic. The BP is traditionally used for the disease and the essential oil of BP has been reported with analgesic and anti-inflammatory effects. The free radical scavenging potential of BP and Au-NPs through XO inhibition supports the use of these samples in various disorders. CA-II is one of the forms of human alpha carbonic anhydrases accelerating reversible hydration of carbon dioxide. Acetazolamide is one of the inhibitors of CA-II and indicated as antiepileptic and diuretics. The diuretic and antiepileptic actions of BP are strongly attributed to the CA-II inhibition. In conclusion, the BP and Au-NPs are the significant urease, XO, and CA-II inhibitors and are responsible to act as remedy for GIT disorders, urinary tract infections, anti-inflammatory, antioxidant, anticonvulsant, and diuretics due to the antagonistic effect of these mentioned enzymes. Moreover, the current study provides a strong scientific background to different folklores of BP.

5 Conclusion

In order to remove and stabilize hazardous solvents, the Au-NPs have been produced utilizing the *B. persicum* alcohol seed extract using the green process. Besides, the nanoparticles were mostly reported in the size of 25–50 nm. FTIR analysis indicated the possible involvement of carbonyl and other groups in the reduction process and may be carboxylate ions act as shielding agents, whereas EDX data showed the presence of neutral gold Au atoms. More concentrated salt solution, low pH, and high temperature will destabilize the Au-NPs as revealed from UV-Vis data. Moreover, the Au-NPs exhibit little antifungal activity along with significant enzyme inhibitory activity.

Acknowledgment: The authors would like to thank the Higher Education Commission of Pakistan. The work is funded by grant number 14-MED333-10 from the National Science, Technology and Innovation Plan (MAARIFAH), National Science, Technology and Innovation Plan (MAARIFAH), the King Abdul-Aziz City for Science and Technology (KACST), Kingdom of Saudi Arabia. We thank the Science and Technology Unit at Umm Al-Qura University for their continued logistic support.

Funding information: The work is funded by grant number 14-MED333-10 from the National Science, Technology and Innovation Plan (MAARIFAH), National Science, Technology and Innovation Plan (MAARIFAH), the King Abdul-Aziz City for Science and Technology (KACST), Kingdom of Saudi Arabia.

Author contributions: Omar Bahattab, Ibrahim Khan, Sami Bawazeer, Abdur Rauf, and Mohammad Nazmul Islam: writing – original draft; Muhammad Nasimullah Qureshi, Mohammad Nazmul Islam, and Yahya S. Al-Awthan: writing – review and editing; Naveed Muhammad, Ajmal Khan, and Muhammad Akram: visualization, project administration; and Talha Bin Emran: resources.

Conflict of interest: One of the authors (Abdur Rauf) is a member of the Editorial Board of Green Processing and Synthesis.

Data availability statement: Available data are presented in the manuscript.

References

[1] Wong S, Karn B. Ensuring sustainability with green nanotechnology. Nanotechnology. 2012;23(29):290201.
[2] Roco MC, Mirkin CA, Hersam MC. Nanotechnology research directions for societal needs in 2020: summary of international study. J Nanopart Res. 2011;13(3):897–919.
[3] Kasthuri J, Kathiravan K, Rajendiran N. Phyllanthin-assisted biosynthesis of silver and gold nanoparticles: a novel biological approach. J Nanopart Res. 2009;11(5):1075–85.
[4] Panyam JL. Biodegradable nanoparticles for drug and gene delivery to cells and tissue. Adv Drug Delivery Rev. 2003;55(3):329–47.
[5] Ma J, Wong H, Kong LB, Peng KW. Biomimetic processing of nanocrystallite bioactive apatite coating on titanium. Nanotechnology. 2003;14(6):619.
[6] O'Neal DP, Hirsch LR, Halas NJ, Payne JD, West JL. Photothermal tumor ablation in mice using near infrared-absorbing nanoparticles. Cancer Lett. 2004;209(2):171–6.
[7] Aslan K, Pérez-Luna VH. Quenched emission of fluorescence by ligand functionalized gold nanoparticles. J Fluorescence. 2004;14(4):401–5.
[8] Zhong W. Nanomaterials in fluorescence-based biosensing. Anal Bioanal Chem. 2009;394(1):47–59.
[9] Narayanan KB, Sakthivel N. Heterogeneous catalytic reduction of anthropogenic pollutant, 4-nitrophenol by silver-bionanocomposite using Cylindrocladium floridanum. Bioresour Technol. 2011;102(22):10737–40.
[10] Rivière C, Boudghène FP, Gazeau F, Roger J, Pons JN, Laissy JP, et al. Iron oxide nanoparticle–labeled rat smooth muscle cells: cardiac MR imaging for cell graft monitoring and quantitation. Radiology. 2005;235(3):959–67.
[11] Moavi J, Buazar F, Sayahi MH. Algal magnetic nickel oxide nanocatalyst in accelerated synthesis of pyridopyrimidine derivatives. Sci Rep. 2021;11(1):6296.

[12] Sepahvand M, Buazar F, Sayahi MH. Novel marine-based gold nanocatalyst in solvent-free synthesis of polyhydroquinoline derivatives: green and sustainable protocol. Appl Organomet Chem. 2020;34(12):e6000.
[13] Buazar F. Impact of biocompatible nanosilica on green stabilization of subgrade soil. Sci Rep. 2019;9(1):15147.
[14] Pastoriza-Santos I, Liz-Marzán LM. Formation of PVP-protected metal nanoparticles in DMF. Langmuir. 2002;18(7):2888–94.
[15] Taleb A, Petit C, Pileni M. Synthesis of highly monodisperse silver nanoparticles from AOT reverse micelles: a way to 2D and 3D self-organization. Chem Mater. 1997;9(4):950–9.
[16] Andreescu D, Eastman C, Balantrapu K, Goia DV. A simple route for manufacturing highly dispersed silver nanoparticles. J Mater Res. 2007;22(9):2488–96.
[17] Rodriguez-Sanchez L, Blanco M, Lopez-Quintela M. Electrochemical synthesis of silver nanoparticles. J Phys Chem B. 2000;104(41):9683–8.
[18] Buazar F, Bavi M, Kroushawi F, Halvani M, Khaledi-Nasab A, Hossieni SA. Potato extract as reducing agent and stabiliser in a facile green one-step synthesis of ZnO nanoparticles. J Exp Nanosci. 2016;11(3):175–84.
[19] Buazar F, Baghlani-Nejazd MH, Badri M, Kashisaz M, Khaledi-Nasab A, Kroushawi F. Facile one-pot phytosynthesis of magnetic nanoparticles using potato extract and their catalytic activity. Starch-Stärke. 2016;68(7–8):796–804.
[20] Buazar F, Sweidi S, Badri M, Kroushawi F. Biofabrication of highly pure copper oxide nanoparticles using wheat seed extract and their catalytic activity: a mechanistic approach. Green Process Synth. 2019;8(1):691–702.
[21] Koopi H, Buazar F. A novel one-pot biosynthesis of pure alpha aluminum oxide nanoparticles using the macroalgae Sargassum ilicifolium: a green marine approach. Ceram Int. 2018;44(8):8940–5.
[22] Saifuddin N, Wong C, Yasumira A. Rapid biosynthesis of silver nanoparticles using culture supernatant of bacteria with microwave irradiation. J Chem. 2009;6(1):61–70.
[23] Bhainsa KC, D'Souza S. Extracellular biosynthesis of silver nanoparticles using the fungus Aspergillus fumigatus. Colloids Surf B Biointerfaces. 2006;47(2):160–4.
[24] Hasna Abdul Salam RP, Kamaraj M, Jagadeeswaran P, Gunalan S, Sivaraj R. Plants: green route for nanoparticle synthesis. I Res J Biol Sci. 2012;1(5):85–90.
[25] Ahamed M, Khan MM, Siddiqui MKJ, AlSalhi MS, Alrokayan SA. Green synthesis, characterization and evaluation of biocompatibility of silver nanoparticles. Phys E: Low-Dimens Syst Nanostruct. 2011;43(6):1266–71.
[26] Rezazadeh NH, Buazar F, Matroodi S. Synergistic effects of combinatorial chitosan and polyphenol biomolecules on enhanced antibacterial activity of biofunctionalized silver nanoparticles. Sci Rep. 2020;10(1):19615.
[27] Moghtader M, Mansori AI, Salari HASAN, Farahmand A. Chemical composition and antimicrobial activity of the essential oil of Bunium persicum Boiss. seed. Iran J Med Aromatic Plants. 2009;25(1):20–8.
[28] Giancarlo S, Rosa LM, Nadjafi F, Francesco M. Hypoglycaemic activity of two spices extracts: Rhus coriaria L. and Bunium persicum Boiss. Nat Product Res. 2006;20(9):882–6.
[29] Salehi P, Mohammadi F, Asghari B. Seed essential oil analysis of Bunium persicum by hydrodistillation-headspace solvent microextraction. Chem Nat Compd. 2008;44(1):111–3.
[30] Foroumadi A, Asadipour A, Arabpour F, Amanzadeh Y. Composition of the essential oil of Bunium persicum (Boiss.) B. Fedtsch. from Iran. J Essent Oil Res. 2002;14(3):161–2.
[31] Jalilzadeh-Amin G, Maham M, Dalir-Naghadeh B, Kheiri F. Effects of Bunium persicum (Boiss.) essential oil on the contractile responses of smooth muscle (an *in vitro* study). Veterinary Research Forum. Vol. 2, Issue 2. Iran: Faculty of Veterinary Medicine, Urmia University; 2011, June. p. 87–96.
[32] Sanei-Dehkordi A, Vatandoost H, Abaei MR, Davari B, Sedaghat MM. Chemical composition and larvicidal activity of Bunium persicum essential oil against two important mosquitoes vectors. J Essent Oil Bear Plants. 2016;19(2):349–57.
[33] Taherkhani P, Noori N, Akhondzadeh Basti A, Gandomi H, Alimohammadi M. Antimicrobial effects of kermanian black cumin (Bunium persicum Boiss.) essential oil in Gouda cheese matrix. J Med Plants. 2015;2(54):76–85.
[34] Hassanzad Azar H, Taami B, Aminzare M, Daneshamooz S. Bunium persicum (Boiss.) B. Fedtsch: an overview on phytochemistry, therapeutic uses and its application in the food industry. J Appl Pharm Sci. 2018;8(10):150–8.
[35] Gholizadeh BS, Buazar F, Hosseini SM, Mousavi SM. Enhanced antibacterial activity, mechanical and physical properties of alginate/hydroxyapatite bionanocomposite film. Int J Biol Macromol. 2018;116:786–92.
[36] Wu P, Bai P, Yan Z, Zhao GX. Gold nanoparticles supported on mesoporous silica: origin of high activity and role of Au NPs in selective oxidation of cyclohexane. Sci Rep. 2016;6(1):1–11.
[37] Dauthal P, Mukhopadhyay M. Prunus domestica fruit extract-mediated synthesis of gold nanoparticles and its catalytic activity for 4-nitrophenol reduction. Ind Eng Chem Res. 2012;51(40):13014–20.
[38] Rauf A, Abu-Izneid T, Rashid U, Alhumaydhi FA, Bawazeer S, Khalil AA, et al. Anti-inflammatory, antibacterial, toxicological profile, and in silico studies of dimeric naphthoquinones from diospyros lotus. BioMed Res Int. 2020;2020:1–10.
[39] Abu-Izneid T, Rauf A, Bawazeer S, Wadood A, Patel S. Anti-dengue, cytotoxicity, antifungal, and in silico study of the newly synthesized 3-*O*-phospo-D-glucopyranuronic acid compound. BioMed Res Int. 2018;2018:1–5.
[40] Shi DH, You ZL, Xu C, Zhang Q, Zhu HL. Synthesis, crystal structure and urease inhibitory activities of Schiff base metal complexes. Inorg Chem Commun. 2007;10(4):404–6.
[41] Islam NU, Jalil K, Shahid M, Muhammad N, Rauf A. Pistacia integerrima gall extract mediated green synthesis of gold nanoparticles and their biological activities. Arab J Chem. 2019;12(8):2310–9.
[42] De Luca V, Del Prete S, Supuran CT, Capasso C. Protonography, a new technique for the analysis of carbonic anhydrase activity. J Enzyme Inhib Med Chem. 2015;30(2):277–82.
[43] Tayab MA, Chowdhury KAA, Jabed M, Mohammed Tareq S, Kamal ATM, Islam MN, et al. Antioxidant-rich woodfordia fruticosa leaf extract alleviates depressive-like behaviors and impede hyperglycemia. Plants. 2021;10(2):287.
[44] Banu N, Alam N, Nazmul Islam M, Islam S, Sakib SA, Hanif NB, et al. Insightful valorization of the biological activities of pani heloch leaves through experimental and computer-aided mechanisms. Molecules. 2020;25(21):5153.

[45] Guha B, Arman M, Islam MN, Tareq SM, Rahman MM, Sakib SA, et al. Unveiling pharmacological studies provide new insights on Mangifera longipes and Quercus gomeziana. Saudi J Biol Sci. 2021;28(1):183–90.
[46] Rahman J, Tareq AM, Hossain M, Sakib SA, Islam MN, Ali M, et al. Biological evaluation, DFT calculations and molecular docking studies on the antidepressant and cytotoxicity activities of cycas pectinata Buch.-Ham. compounds. Pharmaceuticals. 2020;13(9):232.
[47] Guinea J. Global trends in the distribution of Candida species causing candidemia. Clin Microbiol Infect. 2014;20:5–10.
[48] Pappas PG, Lionakis MS, Arendrup MC, Ostrosky-Zeichner L, Kullberg BJ. Invasive candidiasis. Nat Rev Dis Prim. 2018;4(1):1–20.
[49] Dühring S, Germerodt S, Skerka C, Zipfel PF, Dandekar T, Schuster S. Host-pathogen interactions between the human innate immune system and Candida albicans–understanding and modeling defense and evasion strategies. Front Microbiology. 2015;6:625.
[50] Rauf A, Uddin G, Raza M, Patel S, Bawazeer S, Ben Hadda T, et al. Urease inhibition potential of Di-naphthodiospyrol from Diospyros lotus roots. Nat product Res. 2017;31(10):1214–8.
[51] Sidebotham R, Baron J. Hypothesis: helicobacter pylori, urease, mucus, and gastric ulcer. Lancet. 1990;335(8683):193–5.
[52] Johnson DE, Russell RG, Lockatell CV, Zulty JC, Warren JW, Mobley HL. Contribution of Proteus mirabilis urease to persistence, urolithiasis, and acute pyelonephritis in a mouse model of ascending urinary tract infection. Infect Immun. 1993;61(7):2748–54.
[53] Rauf A, Raza M, Saleem M, Ozgen U, Karaoglan ES, Renda G, et al. Carbonic anhydrase and urease inhibitory potential of various plant phenolics using *in vitro* and *in silico* methods. Chem Biodivers. 2017;14(6):e1700024.
[54] Aminzare M, Amiri E, Abbasi Z, Hassanzad Azar H, Hashemi M. Evaluation of *in vitro* antioxidant characteristics of corn starch bioactive films incorporated with bunium persicum and zataria multiflora essential oils. Annu Res Rev Biol. 2017;15(5):1–9.
[55] Islam MN, Rauf A, Fahad FI, Emran TB, Mitra S, Olatunde A, et al. Superoxide dismutase: an updated review on its health benefits and industrial applications. Crit Rev Food Sci Nutr. 2021;1–19.
[56] Slavin YN, Asnis J, Häfeli UO, Bach H. Metal nanoparticles: understanding the mechanisms behind antibacterial activity. J Nanobiotechnology. 2017;15(1):1–20.